

# Pathology Segmentation using Distributional Differences to Images of Healthy Origin

Simon Andermatt, Antal Horváth, Simon Pezold, and Philippe Cattin

Department of Biomedical Engineering, University of Basel, Allschwil, Switzerland

**Abstract.** We present a method to model pathologies in medical data, trained on data labelled on the image level as healthy or containing a visual defect. Our model not only allows us to create pixelwise semantic segmentations, it is also able to create inpaintings for the segmentations to render the pathological image healthy. Furthermore, we can draw new unseen pathology samples from this model based on the distribution in the data. We show quantitatively, that our method is able to segment pathologies with a surprising accuracy and show qualitative results of both the segmentations and inpaintings. A comparison with a supervised segmentation method indicates, that the accuracy of our proposed weakly-supervised segmentation is nevertheless quite close.

## 1 Introduction

Supervised segmentation in medical image analysis is an almost solved problem, where methodological improvements have a marginal effect on accuracy. Such methods depend on a large annotated training corpus, where pixelwise labels have to be provided by medical experts. In practice, such data are expensive to gather. In contrast, weakly labelled data, such as images showing a certain disease are easily obtainable, since they are created on a daily basis in medical practice. We want to take advantage of these data for pathology segmentation, by providing a means to finding the difference between healthy and pathological data distributions. We present a weakly supervised framework capable of pixelwise segmentation as well as generating samples from the pathology distribution.

Our idea is inspired by CycleGAN [10], a recently proposed solution for unpaired image to image translation, where the combination of domain-specific generative adversarial networks (GANs) and so-called cycle consistency allow for robust translation. We call our adaptation PathoGAN and count the following contributions: We formulate a model capable of segmentation based on a single label per training sample. We simultaneously train two generative models, able to generate inpaintings at a localized region of interest to transform an image from one domain to the other. We are able to sample healthy brains as well as sample possible pathologies for a given brain. Furthermore, our method enforces domain-specific information to be encoded outside of the image, which omits adversarial “noise” common to CycleGAN [4] to some degree.

We show the performance of our implementation on 2d slices of the training data of the Brain Tumor Segmentation Challenge 2017 [8,2] and compare our segmentation performance to a supervised segmentation technique [1].

CycleGAN has been previously used to segment by transferring to another target modality, where segmentation maps are available (e.g. [9]), or applied to generate training from cheaply generated synthetic labelmaps [5]. Using a Wasserstein GAN, another method directly estimates an additive visual attribution map [3]. To our knowledge, there has not been a method that jointly learns to segment on one medical imaging modality using only image-level labels and generate new data using GANs for both healthy and pathological cases.

## 2 Methods

### 2.1 Problem Statement

We assume two image domains  $\mathcal{A}$  and  $\mathcal{B}$ , where the former contains only images of healthy subjects and the latter consists of images showing a specific pathology. We seek to approximate the functions  $G_{\mathcal{A}}$  and  $G_{\mathcal{B}}$  that perform the mappings  $(x_{\mathcal{A}}, \delta_{\mathcal{B}}) \mapsto \hat{x}_{\mathcal{B}}$  and  $(x_{\mathcal{B}}, \delta_{\mathcal{A}}) \mapsto \hat{x}_{\mathcal{A}}$ , where  $x_{\mathcal{A}}, \hat{x}_{\mathcal{A}} \in \mathcal{A}$  and  $x_{\mathcal{B}}, \hat{x}_{\mathcal{B}} \in \mathcal{B}$ . Vectors  $\delta_{\mathcal{B}}$  and  $\delta_{\mathcal{A}}$  encode the missing target image information (e.g. the pathology):

$$\hat{x}_{\mathcal{B}} = G_{\mathcal{A}}(x_{\mathcal{A}}, \delta_{\mathcal{B}}), \quad \hat{x}_{\mathcal{A}} = G_{\mathcal{B}}(x_{\mathcal{B}}, \delta_{\mathcal{A}}). \quad (1)$$

In the remaining paper, we use  $X$  and  $Y$  as placeholders for  $\mathcal{A}$  and  $\mathcal{B}$  or  $\mathcal{B}$  and  $\mathcal{A}$  to overcome redundancy due to symmetrical components. We encourage  $G_{\mathcal{A}}, G_{\mathcal{B}}$  to produce results, such that the mappings are realistic (2), bijective (3), specific (4) and that only the affected part in the image is modified (5):

$$G_X(x_X, \delta_Y) \sim Y, \quad (2) \qquad G_Y(x_X, 0) \approx x_X, \quad (4)$$

$$G_Y(G_X(x_X, \delta_Y), \delta_X) \approx x_X, \quad (3) \qquad G_X \approx \arg \min |x_X - G_X(x_X, \delta_Y)|. \quad (5)$$

### 2.2 Model Topology

To fulfill Eqs. (2–5), we adopt the main setup and objective from CycleGAN: we employ two discriminators,  $D_{\mathcal{A}}$  and  $D_{\mathcal{B}}$  together with generators  $G_{\mathcal{A}}$  and  $G_{\mathcal{B}}$  to perform the translation from domain  $\mathcal{A}$  to  $\mathcal{B}$  and vice versa, formulating two generative adversarial networks (GANs) [6]. In both directions, the respective discriminator is trained to distinguish a real image from the output of the generator, whereas the generator is incentivized to generate samples that fool the discriminator.

**Residual Generator** In order to segment pathologies, we seek to only modify a certain part of the image. In contrast to CycleGAN, we model the transformation  $G$  from one domain to the other as a residual or inpainting  $p$  which is exchanged with part  $l$  of the original image. We achieve this by letting generator  $G_X$  directly

estimate  $n + 1$  featuremaps  $r_X$ , where  $n$  is the number of image channels used. We obtain labelmap  $l_X$  and inpaintings  $p_X$ , activating  $r_Y^{(0)}$  with a sigmoid and each  $r_X^{(i)}$  with a tanh activation:

$$l_X = S\left(r_X^{(0)} + \epsilon\right), \quad p_X^{(i-1)} = \tanh\left(r_X^{(i)}\right), \quad (6)$$

where  $S(y) = \frac{1}{1+e^{-y}}$  and  $i > 0$ . With  $\epsilon \sim \mathcal{N}(0, I)$ , we turn  $r_X^{(0)} + \epsilon$  into samples from  $\mathcal{N}(r_X^{(0)}, I)$  using the reparameterization trick [7]. This allows reliable calculations of  $l_X$  only for large absolute values of  $r_X^{(0)}$ , forcing  $l_X$  to be binary and intensity information to be encoded in the inpaintings. We set  $\epsilon$  to zero during testing. From  $l_X$  and  $p_X$  we compute the translated result  $\hat{x}_Y$ , supposedly in domain  $Y$  now:

$$\hat{x}_Y = l_X \odot p_X + (1 - l_X) \odot x_X.$$

In the following, we detail the computation of  $r$  for the two possible translation directions. Both translation pathways are visualized in Fig. 1.

**$\mathcal{A} \rightarrow \mathcal{B}$**  To map from healthy to pathological data, we estimate  $r_{\mathcal{A}}$  (and thus  $l_{\mathcal{A}}, p_{\mathcal{A}}$ ) using a variational autoencoder (VAE) [7]. First, we employ encoders  $\Gamma_{\mathcal{A}}$  and  $\Delta_{\mathcal{B}}$  to encode anatomical information around and inside the pathological region:

$$\gamma_{\mathcal{A}} = \Gamma(x_{\mathcal{A}}), \quad \delta_{\mathcal{B}} = \Delta(l'_{\mathcal{B}} \odot x'_{\mathcal{B}}),$$

where  $x_{\mathcal{A}}$  is our healthy image,  $l'_{\mathcal{B}}$  and  $x'_{\mathcal{B}}$  are the labelmap and pathological image of the previous transformation and  $\delta_{\mathcal{B}}, \gamma_{\mathcal{A}} \sim \mathcal{N}(0, I)$ . If  $l'_{\mathcal{B}}$  and  $x'_{\mathcal{B}}$  are not available because  $x_{\mathcal{A}}$  is a real healthy image, we simply sample  $\delta_y$ . Finally, a decoder  $E_{\mathcal{A}}$  is applied to  $\gamma_{\mathcal{A}}$  and  $\delta_{\mathcal{B}}$ :

$$r_{\mathcal{A}} = E_{\mathcal{A}}(\gamma_{\mathcal{A}}, \delta_{\mathcal{B}}).$$

**$\mathcal{B} \rightarrow \mathcal{A}$**  To generate healthy samples from pathological images, we use a generator  $E_{\mathcal{B}}$  directly on the input as introduced in [10] and estimate  $r$  directly:

$$r_{\mathcal{B}} = E_{\mathcal{B}}(x_{\mathcal{B}}).$$

Here, we omit  $\delta_{\mathcal{A}}$ , since the location and appearance of missing healthy tissue can be inferred from  $x_{\mathcal{B}}$ . We also omit using an encoding bottleneck due to possible information loss and less accurate segmentation.

### 2.3 Objective

To train this model, a number of different loss terms are necessary. In the following, we explain the individual components using  $\hat{\cdot}$  and  $\tilde{\cdot}$  to denote results from the translated and reconstructed images respectively (e.g. mapping  $x_X$  into  $Y$  results in  $\hat{x}_Y$ , translating it back results in  $\tilde{x}_X$ ). We use  $\lambda$ , to weight the contribution of different loss terms.

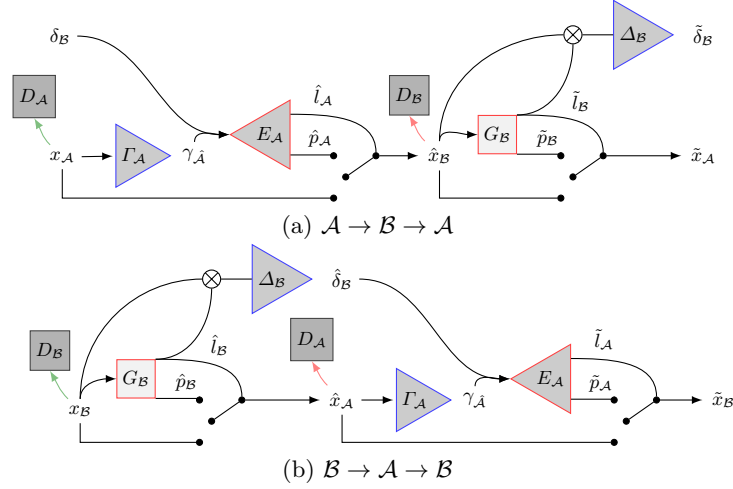


**Fig. 1.** Proposed architecture: *top to bottom*: directions  $\mathcal{A} \rightarrow \mathcal{B} \rightarrow \mathcal{A}$  and  $\mathcal{B} \rightarrow \mathcal{A} \rightarrow \mathcal{B}$ ;  $x_{\mathcal{A}}, x_{\mathcal{B}}$  are samples from the two data distributions  $\mathcal{A}, \mathcal{B}$  and  $\delta_{\mathcal{B}} \sim \mathcal{N}(0, I)$ . Red and blue triangles depict decoder and encoder networks. A red square illustrates a simple generator.  $\Delta_{\mathcal{B}}, \Gamma_{\mathcal{A}}$  encode features inside and outside the pathological region.  $\Delta_{\mathcal{B}}, \Gamma_{\mathcal{A}}$  and  $E_{\mathcal{A}}$  form a variational autoencoder. For  $G_{\mathcal{B}}$ , information about the missing healthy structure is completely inferred from the surroundings.

**CycleGAN** As in CycleGAN [10], we formulate a least squares proxy GAN loss, which we minimize with respect to  $G_X$  and maximize with respect to  $D_Y$ :

$$\mathcal{L}_{\text{GAN}}(D_Y, G_X, x_X, x_Y) = \mathbb{E}[(D_Y(x_Y))^2] + \mathbb{E}[(1 - D_Y(G_X(x_X, \delta_Y)))^2], \quad (7)$$

Likewise, to make mappings reversible, we add the cycle consistency loss:

$$\mathcal{L}_{\text{CC}}(G_X, G_Y, x_X) = \lambda_{\text{CC}} \|G_Y(G_X(x_X, \delta_Y), \delta_X) - x_X\|_1. \quad (8)$$

$\mathcal{L}_{\text{GAN}}$  and  $\mathcal{L}_{\text{CC}}$  encourage the properties defined in Eqs. (2) and (3).

**Variational Autoencoder** A variational autoencoder (VAE) is trained by minimizing the KL-divergence of the distribution  $q(z|x)$  of encoding  $z$  to some assumed distribution and the expected reconstruction error  $\log p(x|z)$ , where  $x$  is the data. In contrast to a classical VAE, we use two distinct encoding vectors  $\gamma_{\mathcal{A}}$  and  $\delta_{\mathcal{B}}$ , encoding the healthy and the pathological part, and produce two separate results, the labelmap  $l_{\mathcal{A}}$  and the inpainting  $p_{\mathcal{A}}$ . We directly calculate the KL-divergence for our two encodings:

$$\mathcal{L}_{\text{KL}}(G_{\mathcal{A}}, G_{\mathcal{B}}, x_{\mathcal{A}}, x_{\mathcal{B}}) = \text{KL}[q(\gamma_{\mathcal{A}}|x_{\mathcal{A}})|\mathcal{N}(0, I)] + \text{KL}[q(\delta_{\mathcal{B}}|x_{\mathcal{B}}, \hat{l}_{\mathcal{B}})|\mathcal{N}(0, I)]. \quad (9)$$

For the expected reconstruction error, we assume that  $l$  and  $p$  follow approximately a Bernoulli and a Gaussian distribution ( $\mathcal{N}(\mu, I)$ ). We selectively penalize

the responsible encoding, by using separate loss functions for the residual region and the rest. Unfortunately, we only ever have access to the ground truth of one of these regions, since we do not use paired data. We solve this, by using the relevant application in the network, where individual ground truths are available, to calculate the approximation of the marginal likelihood lower bound:

$$\begin{aligned} \mathcal{L}_{\text{VAE}}(G_X, G_Y, x_X, x_Y) = \\ - \frac{\lambda_{\text{VAE}}}{N} \sum_{m=1}^N (\log p(\tilde{l}_Y | \gamma_X, \delta_Y) + \log p(\hat{p}_X | \gamma_X) + \log p(\tilde{p}_Y | \delta_Y)), \end{aligned} \quad (10)$$

where  $\hat{p}_X$  denotes the inpainting used to translate the original image  $x_X$  to domain  $Y$  and  $N$  is the total number of pixels.  $\tilde{p}_X$  is the inpainting produced when translating an already translated image  $\hat{x}_X$  that originated from  $Y$  back to that domain. Similarly,  $\hat{l}_X$  and  $\tilde{l}_X$  denote the respective labelmaps:

$$\log p(\hat{p}_X | \gamma_X) = \frac{\|(1 - \hat{l}_X)(\hat{p}_X - x_X)\|_2}{\omega_1}, \log p(\tilde{p}_X | \delta_Y) = \frac{\|\tilde{l}_Y(\tilde{p}_X - x_Y)\|_2}{\omega_2} \quad (11)$$

where  $\omega_1 = \frac{(\sum(1 - \hat{l}_X) + \varepsilon)}{N}$  and  $\omega_2 = \frac{(\sum(\tilde{l}_Y) + \varepsilon)}{N}$  are considered constant during optimization, with  $\varepsilon > 0$ . Finally, we use the labelmap produced by the other generator responsible for the opposite transformation  $\hat{l}_Y$  as ground truth for  $\tilde{l}_X$ , where we consider  $\hat{l}_Y$  constant in this term:

$$\log p(\tilde{l}_X | \gamma_X, \delta_Y) = \hat{l}_Y \log \tilde{l}_X + (1 - \hat{l}_Y) \log(1 - \tilde{l}_X). \quad (12)$$

To restrict the solution space of our model, we use  $\mathcal{L}_{\text{VAE}}$  for both directions.

**Identity Loss** We apply an identity loss [10] on labelmap  $l_{X,x_Y}$  which results from feeding  $G_X$  with the wrong input  $x_Y$ . In this case  $G_X$  should not change anything, since the input is already in the desired domain  $Y$ :

$$\mathcal{L}_{\text{Idt}}(G_X, x_Y) = \lambda_{\text{Idt}} \|l_{X,x_Y}\|_1. \quad (13)$$

**Relevancy Loss** By now, we have defined all necessary constraints for a successful translation between image domains. The remaining constraints restrict the location and amount of change,  $l_X$ . Fulfilling Eq. (5), we want to entice label map  $l_X$  to be only set at locations of a large difference between inpainting  $p_X$  and image  $x_X$  and penalize large label maps in general:

$$\mathcal{L}_{\text{R}}(G_X, x_X) = \lambda_{\text{R}} \left[ \|\log(1 - l_X^2)\|_1 - \frac{\|l_X(x_X - p_X)\|_1}{\|l_X\|_1} \right]. \quad (14)$$

In order to not reward exaggerated pathology inpaintings, we consider  $(x_X - p_X)$  constant in this expression.

**Full PathoGAN Objective** combining all loss terms for direction  $X$  to  $Y$  as  $\mathcal{L}_{X \rightarrow Y}$ , we can finally define:

$$\mathcal{L}_{X \rightarrow Y} = \mathcal{L}_{\text{GAN}} + \mathcal{L}_{\text{CC}} + \mathcal{L}_{\text{VAE}} + \mathcal{L}_{\text{Idt}} + \mathcal{L}_{\text{R}}, \quad (15)$$

$$\mathcal{L}_{\text{PathoGAN}} = \mathcal{L}_{\mathcal{A} \rightarrow \mathcal{B}} + \mathcal{L}_{\mathcal{B} \rightarrow \mathcal{A}} + \lambda_{\text{KL}} \mathcal{L}_{\text{KL}}(x_{\mathcal{A}}, x_{\mathcal{B}}). \quad (16)$$

## 2.4 Training

We include all training patients of Brats2017 and normalize each brain scan to follow  $\mathcal{N}(0, 1/3)$ , excluding zero voxels, and clip the resulting intensities to  $[-1, 1]$ . We select all slices from 60 to 100. In order to create two distinct datasets and relying on the manual segmentations, we label slices without pathology as *healthy*, with more than 20 pixels segmented as *pathological* slices, and discard the rest. For training, we select 1500 unaffected and 6000 pathological slices from a total of 1755 and 9413 respectively<sup>1</sup>.

Since the BratS evaluation is volumetric and comparing performance is difficult, we also train a supervised segmentation technique on our data. We chose MDGRU [1] for this task, a multi-dimensional recurrent neural network, due to code availability and consistent state-of-the-art performance on different datasets.

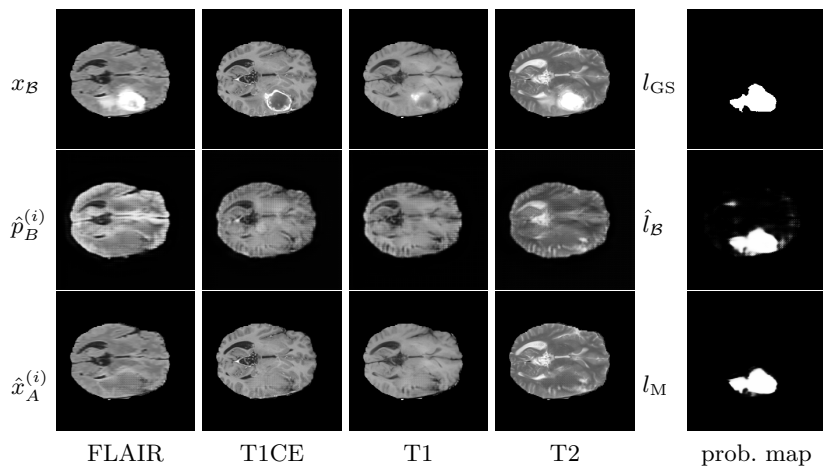


**Fig. 2.** Qualitative Results of one testing data example. *Left columns, top to bottom:* the four available image channels  $x_B^{(i)}$ , the generated inpaintings  $\hat{p}_B^{(i)}$  and the translated images  $\hat{x}_A^{(i)}$ . *Right column, top to bottom:* The manual segmentation  $l_{\text{GS}}$ , the probability maps  $\hat{l}_B$  from PathoGAN and  $l_M$  from MDGRU for whole tumor.

<sup>1</sup> Thus we would like to stress that the manual segmentations were only used to create the two image domains, but not for the actual training.

### 3 Results

We train PathoGAN<sup>2</sup> for 119 epochs using batches of 4 and  $\lambda_{KL} = 0.1, \lambda_R = 0.5, \lambda_{Idt} = 1, \lambda_{CC} = 5$  and  $\lambda_{VAE} = 1$ . We trained MDGRU<sup>3</sup> as defined in [1], using batches of 4 and 27 500 iterations. During training of both PathoGAN and MDGRU, we use weak data augmentation [1]. Table 1 shows the results on the pathological training and test data. On the left, Fig. 2 shows an exemplary sample from the testset, with generated inpaintings and translation result. On the right, we provide the generated labelmap together with the manual label for “whole tumor” and the computed segmentation with MDGRU. Details on the used architecture and training procedure as well as further qualitative samples are described in the supplementary material.

**Table 1.** Segmentation Results. *Columns:* Dice, 95th percentile Hausdorff distance (HD95), average Hausdorff distance (AVD) and volumetric Dice per-patient (Dice PP) by stacking all evaluated slices. *Rows:* Scores are shown as mean $\pm$ std(median) for PathoGAN (proposed) and MDGRU, applied to training (Tr) and testing (Te) data.

	Dice (in %)	HD95 (in pixel)	AVD (in pixel)	Dice PP (in %)
PathoGAN (Tr)	72.4 $\pm$ 24.4(81.0)	40.6 $\pm$ 30.7(38.0)	10.3 $\pm$ 15.4(4.7)	77.4 $\pm$ 14.4(81.2)
PathoGAN (Te)	72.9 $\pm$ 23.8(81.4)	39.4 $\pm$ 29.9(37.6)	9.4 $\pm$ 13.7(4.6)	77.4 $\pm$ 14.4(81.7)
MDGRU (Tr)	87.8 $\pm$ 20.0(94.4)	3.7 $\pm$ 9.7(1.0)	1.0 $\pm$ 4.7(0.2)	90.8 $\pm$ 8.8(93.3)
MDGRU (Te)	86.3 $\pm$ 21.3(93.6)	3.9 $\pm$ 9.5(1.0)	1.1 $\pm$ 4.9(0.2)	90.6 $\pm$ 9.5(93.1)

### 4 Discussion

The results in Fig. 2 indicate that our relative weighting of the two inpainting reconstruction losses results in better reconstruction inside the tumor region than outside. The labelmaps of the supervised method compared to ours in Fig. 2 show great agreement, and both are relatively close to the gold standard. As the 95th-percentile and average Hausdorff measures in Table 1 show, there are some outliers in our proposed method, due to its weakly-supervised nature. The Dice score is about 10% smaller for both the per-slice as well as the per-patient case, given no labels are provided. It is important to remember that we segment with the only criterion of being not part of the healthy distribution, which could vary from the subjective measures used to manually segment data. The increase in accuracy and decrease in standard deviation in the per-patient case for both

<sup>2</sup> Our implementation is based on <https://github.com/junyanz/pytorch-CycleGAN-and-pix2pix>.

<sup>3</sup> We use the implementation of MDGRU at <https://github.com/zubata88/mdgru>.

methods is most likely caused by the inferior segmentation performance in slices showing little pathology. The per-patient Dice of the supervised method is in the range of the top methods of BraTS 2017. Although not directly comparable, this suggests that we can use our computed supervised scores as good reference to compare our results to.

We did only scratch the surface on the possible applications of our proposed formulation. Future work will include unaffected samples that are actually healthy. Furthermore, the model architecture could be drastically simplified using one discriminator for both directions, allowing for larger generator networks as well as using multiple discriminators at different scales to find inpaintings that are not just locally but also globally consistent with the image. A restriction to slices is unfortunate but necessary due to memory requirements. A generalisation of our approach to volumetric data would make it feasible for more real clinical applications.

*Conclusion* We presented a new generative pathology segmentation model capable of handling a plethora of tasks: First and foremost, we presented a weakly supervised segmentation method for pathologies in 2D medical images, where it is only known if the image is affected by the pathology. Furthermore, we were able to sample from both our healthy as well as our pathology model. We showed qualitatively and quantitatively, that we are able to produce compelling results, motivating further research towards actual clinical applications of PathoGAN.

## References

1. Andermatt, S., Pezold, S., Cattin, P.: Multi-dimensional Gated Recurrent Units for the Segmentation of Biomedical 3D-Data. In: International Workshop on Large-Scale Annotation of Biomedical Data and Expert Label Synthesis. pp. 142–151. Springer (2016)
2. Bakas, S., Akbari, H., Sotiras, A., Bilello, M., Rozycki, M., Kirby, J., Freymann, J., Farahani, K., Davatzikos, C.: Advancing The Cancer Genome Atlas glioma MRI collections with expert segmentation labels and radiomic features. *Nature Scientific Data* (2017), [in press]
3. Baumgartner, C.F., Koch, L.M., Tezcan, K.C., Ang, J.X., Konukoglu, E.: Visual feature attribution using wasserstein gans. *arXiv preprint arXiv:1711.08998* (2017)
4. Chu, C., Zhmoginov, A., Sandler, M.: CycleGAN, a Master of Steganography. *arXiv:1712.02950 [cs, stat]* (Dec 2017)
5. Fu, C., Lee, S., Ho, D.J., Han, S., Salama, P., Dunn, K.W., Delp, E.J.: Fluorescence microscopy image segmentation using convolutional neural network with generative adversarial networks. *arXiv preprint arXiv:1801.07198* (2018)
6. Goodfellow, I., Pouget-Abadie, J., Mirza, M., Xu, B., Warde-Farley, D., Ozair, S., Courville, A., Bengio, Y.: Generative adversarial nets. In: *Advances in neural information processing systems*. pp. 2672–2680 (2014)
7. Kingma, D.P., Welling, M.: Stochastic gradient vb and the variational auto-encoder. In: *Second International Conference on Learning Representations* (2014)
8. Menze, B.H., Jakab, A., Bauer, S., et al: The Multimodal Brain Tumor Image Segmentation Benchmark (BRATS). *IEEE Transactions on Medical Imaging* 34(10), 1993–2024 (Oct 2015)

9. Tsaftaris, S.A.: Adversarial image synthesis for unpaired multi-modal cardiac data. In: *Simulation and Synthesis in Medical Imaging: Second International Workshop, SASHIMI 2017, Held in Conjunction with MICCAI 2017*. p. 3. Springer (2017)
10. Zhu, J.Y., Park, T., Isola, P., Efros, A.A.: Unpaired Image-To-Image Translation Using Cycle-Consistent Adversarial Networks. pp. 2223–2232 (2017)



## C Additional Visual Results

Additional visual results were randomly selected with the command `ls testfolder | shuf | tail -n 20` and are shown in Figs 3 to 22. The first row in the figures shows the available sequences (FLAIR, T1CE, T1, T2) and the manual segmentation, the second the respective generated inpaintings and probability map and the last row shows on the left the four final translations for each sequence as well as the generated probability map using the supervised MDGRU[1] reference method.

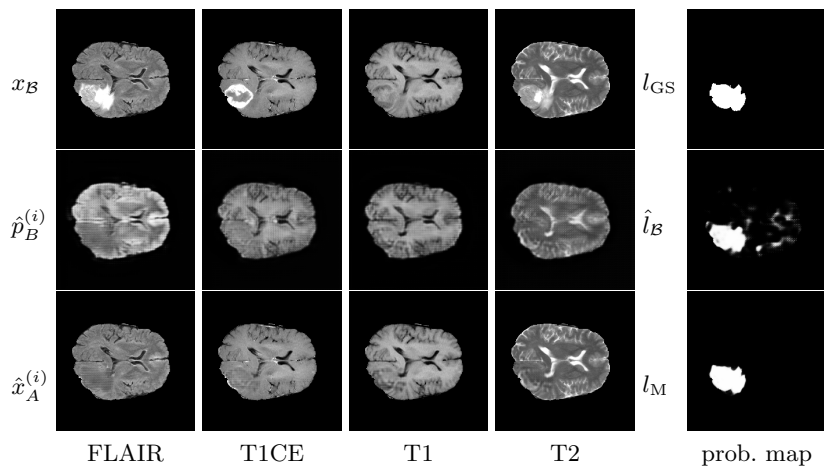


**Fig. 3.** Random sample: HGG-Brats17\_TCIA\_335\_1-73

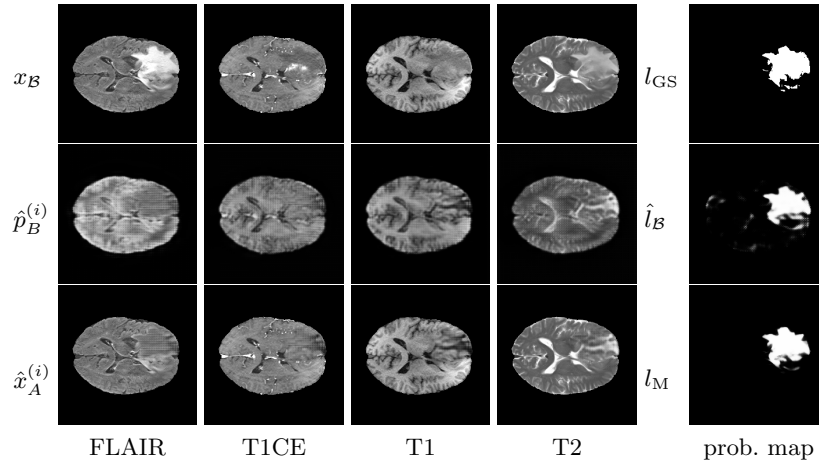


**Fig. 4.** Random sample: HGG-Brats17\_CBICA\_AQY\_1-70

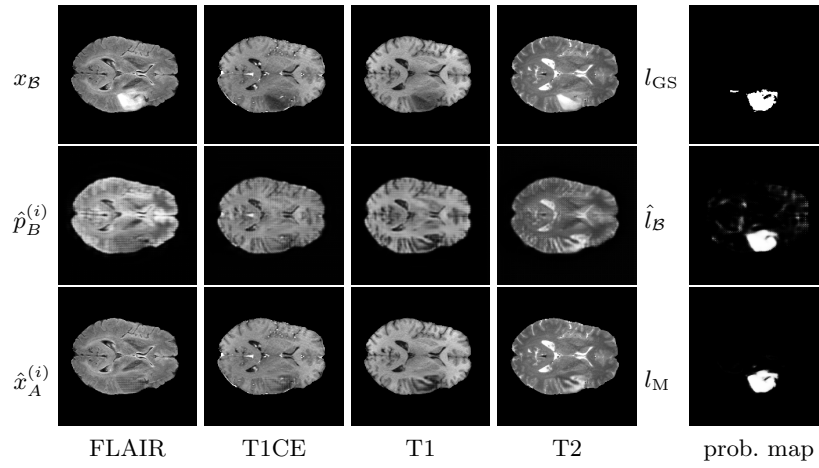


**Fig. 5.** Random sample: HGG-Brats17\_CBICA\_AAG\_1-71

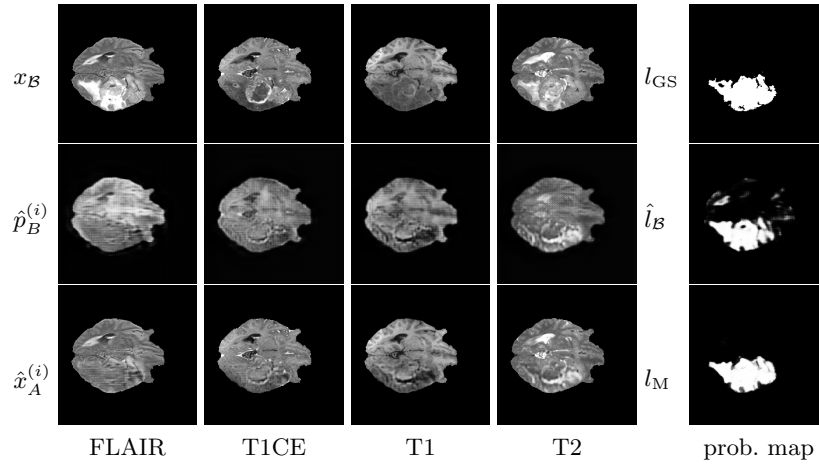


**Fig. 6.** Random sample: HGG-Brats17\_CBICA\_ABO\_1-67

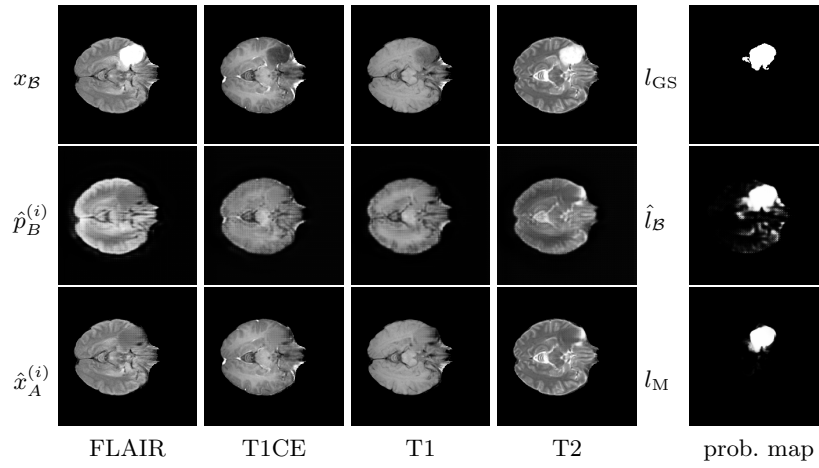


**Fig. 7.** Random sample: LGG-Brats17\_TCIA\_630\_1-60

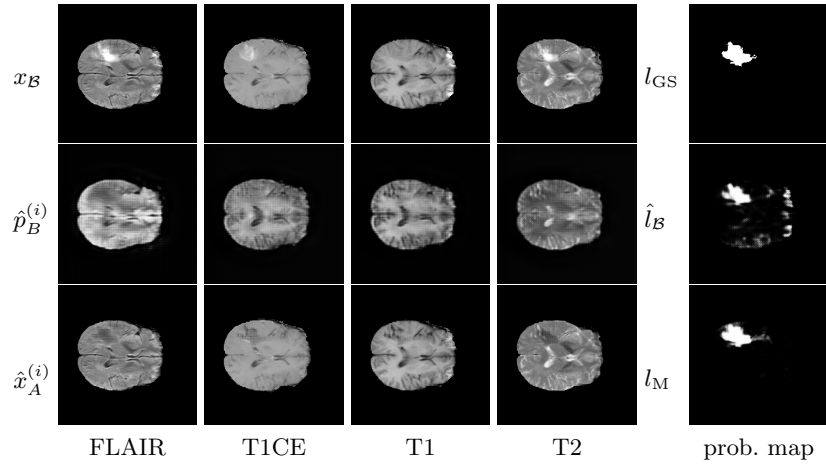


**Fig. 8.** Random sample: HGG-Brats17\_TCIA\_278\_1-83

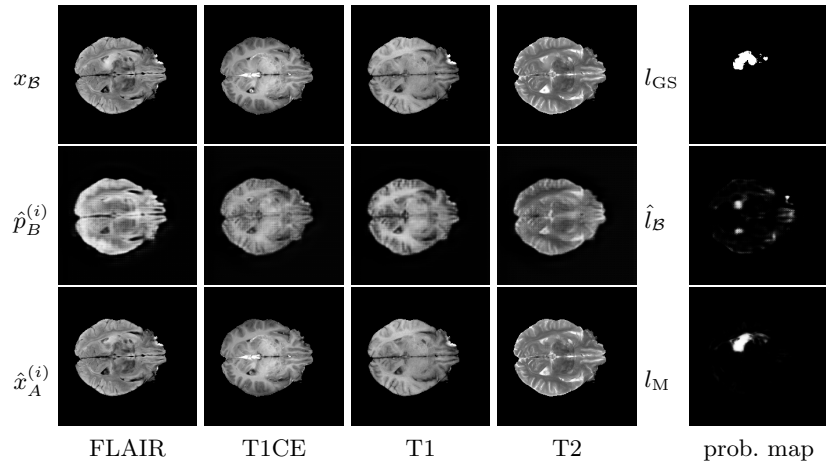


**Fig. 9.** Random sample: LGG-Brats17\_TCIA\_177\_1-64

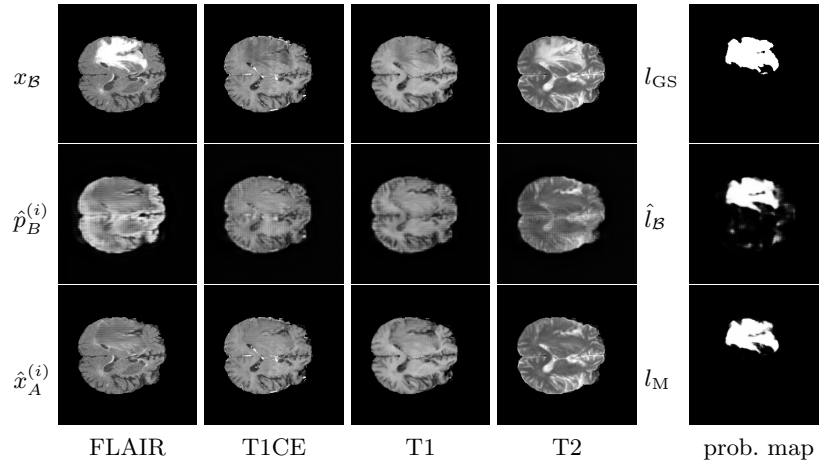


**Fig. 10.** Random sample: HGG-Brats17\_TCIA\_471\_1-76

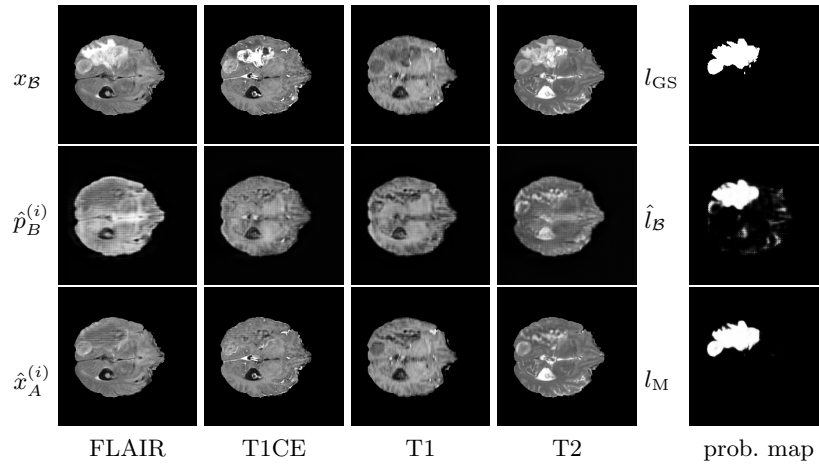


**Fig. 11.** Random sample: HGG-Brats17\_TCIA\_296\_1-62

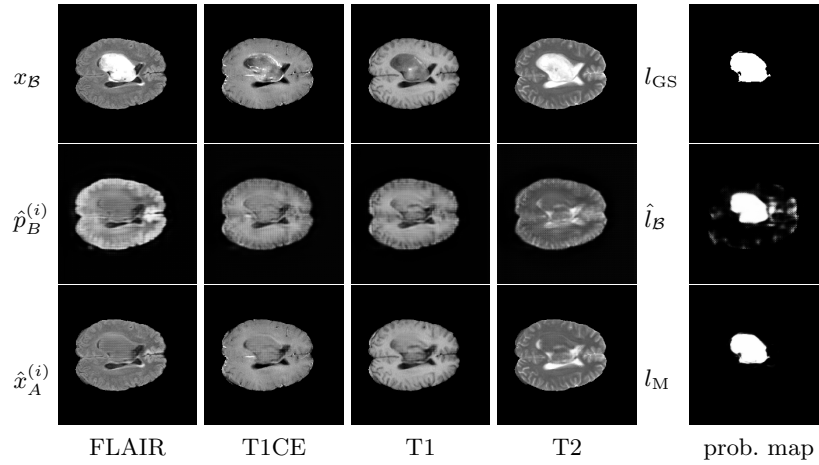


**Fig. 12.** Random sample: HGG-Brats17\_TCIA\_460\_1-91

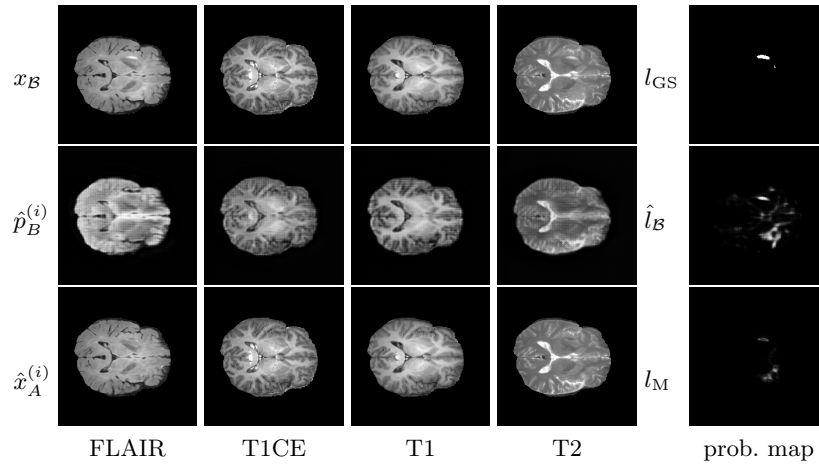


**Fig. 13.** Random sample: HGG-Brats17\_TCIA\_198\_1-68

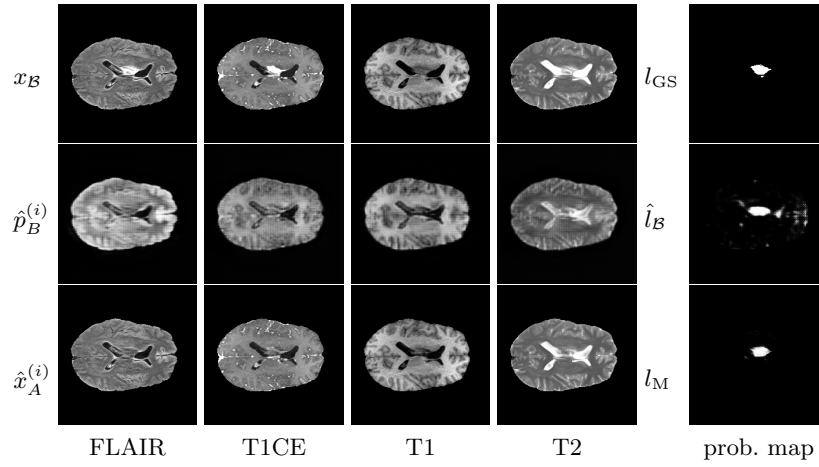


**Fig. 14.** Random sample: HGG-Brats17\_CBICA\_AOO\_1-77

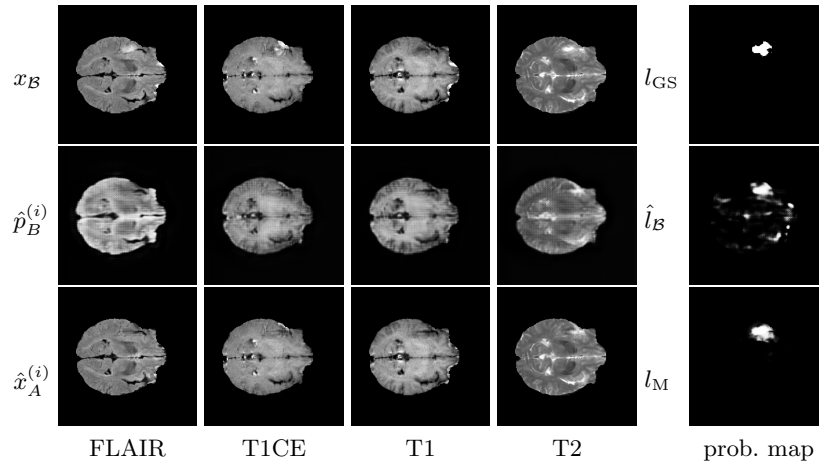


**Fig. 15.** Random sample: HGG-Brats17\_TCIA\_218\_1-65

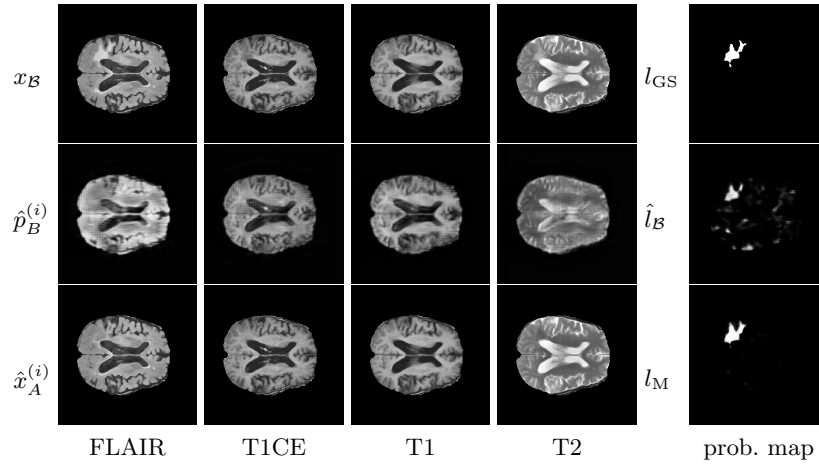


**Fig. 16.** Random sample: HGG-Brats17\_TCIA\_208\_1-78

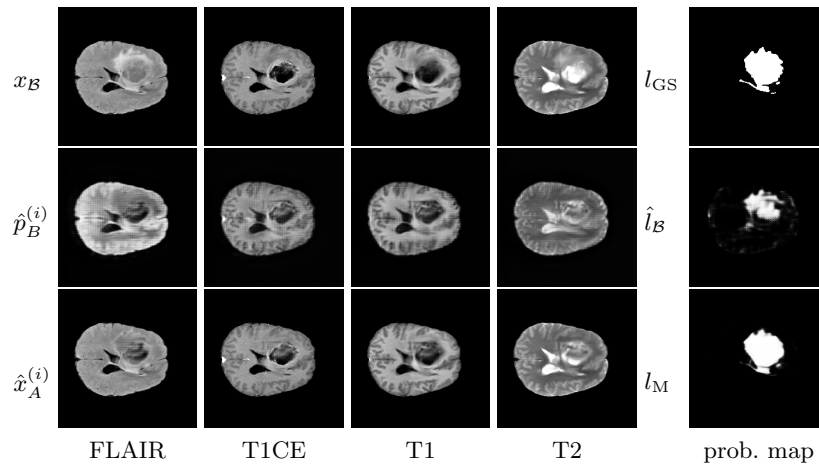


**Fig. 17.** Random sample: HGG-Brats17\_TCIA\_606\_1-83

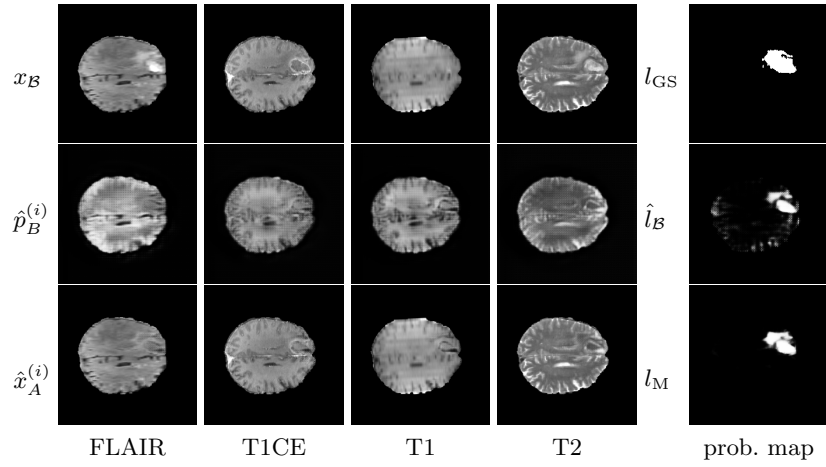


**Fig. 18.** Random sample: HGG-Brats17\_2013\_4\_1-94

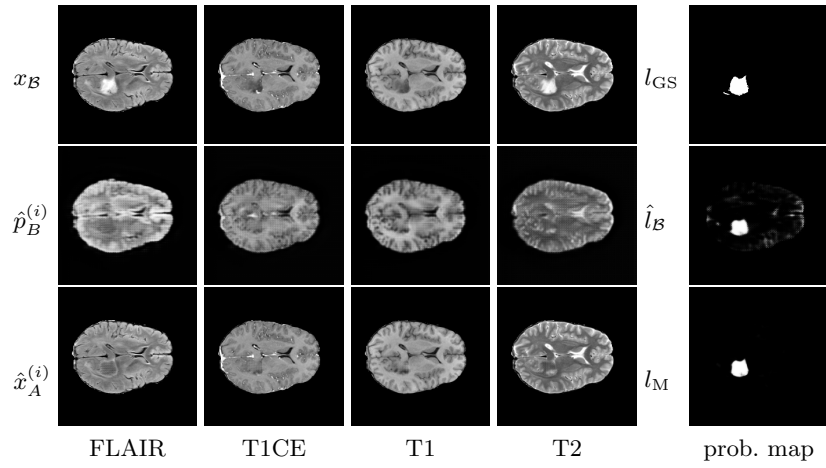


**Fig. 19.** Random sample: LGG-Brats17\_TCIA\_645\_1-79

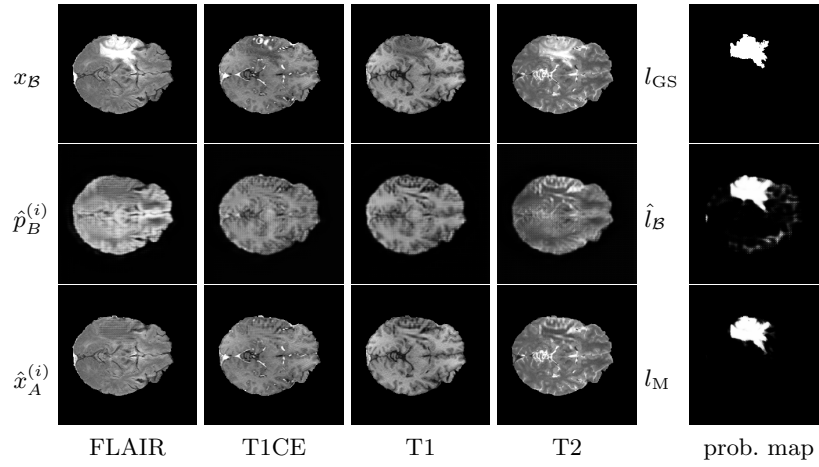


**Fig. 20.** Random sample: HGG-Brats17\_CBICA\_ANI\_1-63

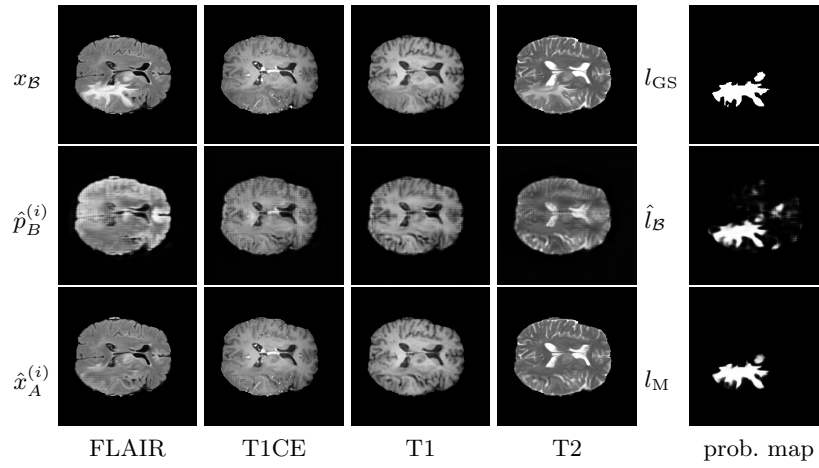


**Fig. 21.** Random sample: HGG-Brats17\_TCIA\_332\_1-79

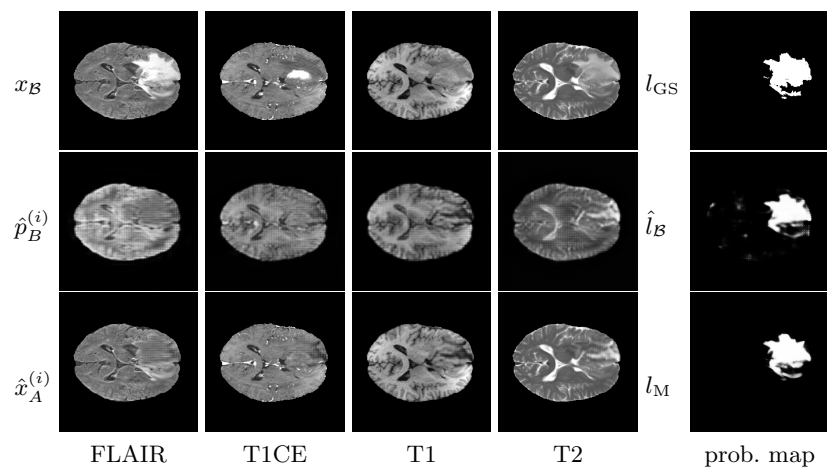


**Fig. 22.** Random sample: HGG-Brats17\_CBICA\_AQY\_1-69